

saw a ball of excess chain segments at the relaxing end until about 100 s (25).

Tube deformation and microscopic elasticity were also observed (Fig. 3B). After the loop was drawn, the bead was rapidly moved away from the loop, pulling the chain taut. This increased tension in the chain squeezed the loop down, deforming the original tube with an applied stress. The entangled polymers that form the constraint were deformed until they balanced the applied stress. After the bead was stopped, the stress applied by the loop decreased as excess chain segments diffused in from the relaxing free end and relieved the tension. With this reduction in stress, the loop grew back to its initial size. In contrast, loops formed in Newtonian fluids always decreased in time. Thus, we have shown the deformation of a tube with an applied stress and its subsequent recovery when the stress is relieved.

The experimental techniques presented in this paper allow for direct observation and controlled deformation of single DNA molecules. Using optical tweezers, one can go beyond passive observations of the Brownian dynamics of polymers by driving the dynamics with forces and stresses applied on the microscopic level of single chains. Quantitative measurements of the excess chain segment diffusion and tube deformation are examples of studies that are now possible. These techniques should allow detailed investigations of the microscopic origin of viscoelastic behavior and other collective effects displayed by solutions of entangled polymers.

## REFERENCES AND NOTES

- J. D. Ferry, *Viscoelastic Properties of Polymers* (Wiley, New York, ed. 3, 1980).
- P. G. de Gennes, *J. Chem. Phys.* **55**, 572 (1971); *Scaling Concepts in Polymer Physics* (Cornell Univ. Press, Ithaca, NY, 1979); *Phys. Today* **36** (no. 6), 33 (June 1983).
- S. F. Edwards, *Proc. Phys. Soc. London* **92**, 9 (1967).
- P. G. de Gennes, *Macromolecules* **9**, 587 (1976).
- M. Doi and S. F. Edwards, *J. Chem. Soc. Faraday Trans. 2* **74**, 1789 (1978); *ibid.*, p. 1802.
- , *The Theory of Polymer Dynamics* (Clarendon, Oxford, 1986).
- T. Lodge, N. Rotstein, S. Prager, *Adv. Chem. Phys.* **79**, 1 (1990).
- J. S. Higgins and J. E. Roots, *J. Chem. Soc. Faraday Trans.* **81**, 757 (1985).
- D. Richter *et al.*, *Phys. Rev. Lett.* **64**, 1389 (1990).
- T. Russell *et al.*, *Nature* **365**, 235 (1993).
- S. Chu, *Science* **253**, 861 (1991).
- T. T. Perkins, S. R. Quake, D. E. Smith, S. Chu, *ibid.* **264**, 822 (1994).
- P. J. Hagerman, *Annu. Rev. Biophys. Biophys. Chem.* **17**, 265 (1988).
- R. Pecora, *Science* **251**, 893 (1991).
- The dye used was YOYO-1 (Molecular Probes, Inc.). For technical reference, see H. S. Rye *et al.*, *Anal. Biochem.* **208**, 144 (1993).
- S. B. Smith, P. K. Aldridge, J. B. Callis, *Science* **243**, 203 (1989); D. C. Schwartz and M. Koval, *Nature* **338**, 520 (1989).
- We prepared the DNA by allowing 12.5 nM of a 28-base pair (bp) oligonucleotide (Stanford University Protein and Nucleic Acid Facility, Stanford,

- CA) complementary to one end of  $\lambda$ -phage DNA to react with an equal molar amount of  $\lambda$ -phage DNA (Gibco BRL) for 24 hours at 25°C in 1X ligase buffer. The DNA was then ligated for 12 hours and purified in a Centricon-100 (Amicon, Beverly, MA) microconcentrator. The oligonucleotide left a specific 16-bp overhang on one end. A second biotinylated oligonucleotide complementary to this 16-bp overhang was attached to the streptavidin-coated polystyrene bead (Interfacial Dynamics, Portland, OR). The modified DNA was then attached to these beads by hybridization.
- Earlier work on manipulation of DNA with optical tweezers was reported by S. Chu and S. Kron [in *International Conference on Quantum Electronics Technical Digest* (Optical Society of America, Washington, DC, 1990), vol. 8, p. 202].
- G. Maret and G. Weill, *Biopolymers* **22**, 2727 (1983).
- A. Ashkin, J. Dziedzic, J. Bjorkholm, S. Chu, *Opt. Lett.* **11**, 288 (1986).
- To reduce photobleaching of the dye and the resulting cleavage of the DNA, we enzymatically scavenged oxygen with glucose oxidase (50  $\mu$ g/ml), 0.1% glucose, and catalase (10  $\mu$ g/ml), as in A. Kishino and T. Yanagida, *Nature* **334**, 74 (1988). Single molecules of DNA could be visualized for up to 45 min.

- S. W. Provencher, *Comput. Phys. Commun.* **27**, 213 (1982).
- In future work, one can overcome this limit by attaching each end of the DNA to a bead and drawing a loop while holding both ends to prevent relaxation of the DNA.
- For example, see H. Wendel and J. Noolandi, *Macromolecules* **15**, 1318 (1982). Similar behavior for chains under tension was considered by E. A. DiMarzio, C. M. Guttman, and J. D. Hoffman [*Faraday Discuss. Chem. Soc.* **68**, 210 (1979)].
- Although this is not visible in the photographic images, this local increase in intensity at the relaxing end was visible in the original video images.
- We acknowledge the generous assistance of J. Spudich, J. Finer, H. Goodson, and G. Nuckolls, including support through National Institutes of Health grant 33289 to J. Spudich. We also acknowledge discussions with G. Fuller, R. Larson, and R. Pecora and the computer code for inverse Laplace transforms from S. Provencher. This work was supported in part by grants from the U.S. Air Force Office of Scientific Research and the National Science Foundation and by an endowment established by Theodore and Frances Geballe.

29 December 1993; accepted 1 April 1994

## Relaxation of a Single DNA Molecule Observed by Optical Microscopy

Thomas T. Perkins, Stephen R. Quake,\*  
Douglas E. Smith, Steven Chu†

Single molecules of DNA, visualized in video fluorescence microscopy, were stretched to full extension in a flow, and their relaxation was measured when the flow stopped. The molecules, attached by one end to a 1-micrometer bead, were manipulated in an aqueous solution with optical tweezers. Inverse Laplace transformations of the relaxation data yielded spectra of decaying exponentials with distinct peaks, and the longest time component ( $\tau$ ) increased with length ( $L$ ) as  $\tau \sim L^{1.66 \pm 0.10}$ . A rescaling analysis showed that most of the relaxation curves had a universal shape and their characteristic times ( $\lambda_t$ ) increased as  $\lambda_t \sim L^{1.65 \pm 0.13}$ . These results are in qualitative agreement with the theoretical prediction of dynamical scaling.

An understanding of the static and dynamic properties of a single isolated chain forms the foundation of polymer physics (1–3). One can then ask questions about the behavior of dilute solutions and eventually consider more concentrated solutions, melts, and gels in which interactions between chains become important. The theoretical approach has involved many techniques: thermodynamic analysis, field theory, scaling, renormalization group theory, and computer simulation (1–3).

Many of the observable static properties of polymers in dilute solutions are well described by scaling relations. If  $A$  is an observable quantity, then  $A \sim M^\nu \sim L^\nu$ , where  $M$  and  $L$  are the molecular weight and length of the polymer and  $\nu$  is the

scaling exponent. The value of  $\nu$  is independent of the local molecular structure of the polymer but does depend on temperature and monomer-solvent interactions (2). De Gennes (4) proposed that these scaling laws can be generalized to dynamical properties such as relaxation and elongation rates, but the experimental verification of this idea has been on less firm ground.

Measurements of rheology, light scattering, and birefringence of bulk samples have been used to study the dynamics of polymer chains (5–7). For example, Keller *et al.* (5) used birefringence measurements to determine the bulk orientational order in regions of dilute polymer solutions. A sharp increase in the birefringence is observed in an extensional flow at a critical strain rate  $d\epsilon_x/dt$ , and a relaxation time  $\tau$  was extracted by assuming that  $(d\epsilon_x/dt)\tau \approx 1$ . In these experiments, it was found that  $\tau \sim \eta L^{1.5}/kT$ , where  $\eta$  is the solvent viscosity,  $k$  is the Boltzmann constant,  $T$  is absolute temper-

Department of Physics, Stanford University, Stanford, CA 94305, USA.

\*Present address: Department of Physics, Oxford University, Oxford OX13NP, United Kingdom.

†To whom correspondence should be addressed.

ature, and the scaling exponent is  $3\nu = 1.5$ , in accordance with the Zimm model for a  $\Theta$ -solvent, in which monomer-monomer interactions are canceled by monomer-solvent interactions (8). Unexpectedly, this result was independent of the "quality" of the solvent as it was varied from a  $\Theta$ -solvent ( $3\nu = 1.5$ ) to a "good" solvent ( $3\nu = 1.8$ ), where there is net swelling of the polymer relative to the  $\Theta$ -solvent. This apparent suppression of excluded volume effects contradicts the theoretically predicted scaling exponent of  $3\nu = 1.8$  (3), which has been observed in intrinsic viscosity measurements (9). However, the relation between birefringence and extension is not entirely clear because it requires independent knowledge of the polarizability and chain conformation. In fact, light scattering experiments suggest that the chains in such flows are only extended by roughly a factor of 2 from their equilibrium size (10). Light scattering has also been used to study the fluctuations of polymers from equilibrium. Measurements of time correlations in scattered light intensities yield a structure factor that is theoretically predicted to scale as a power law with the exponent  $\nu$  (3). For good solvents, the measured exponent is about 0.55 (6, 7), which is slightly smaller than the theoretical value of 0.6. In terms of relaxation scaling exponents, this is an experimental value of  $3\nu = 1.65$  instead of  $3\nu = 1.8$ .

Crothers and Zimm measured the intrinsic viscosity of DNA as a function of molecular weight and determined the scaling exponent to be 0.66 (11). Within the Zimm model, the intrinsic viscosity scales as  $[\eta] \sim L^{3\nu-1}$  (3), and this gives an experimental value of  $3\nu = 1.65$  for chains with molecular weights of up to  $1.3 \times 10^8$  (62.7  $\mu\text{m}$  long). Des Cloizeaux has argued

that the scaling exponent may very slowly approach its theoretical value of  $3\nu = 1.8$  for a good solvent as the chain length increases (12).

Although these traditional methods of experimentation have given much insight, they have an inherent disadvantage: The relaxation properties of a single chain must be inferred from indirect measurements averaged over a macroscopically large number of chains. In addition, the polymer solutions used are not always monodisperse. Finally, in most hydrodynamic flow experiments, the time during which a measurement may be made on a particular volume of sample is short because the fluid element is rapidly carried away by the flow (5). We avoided these problems by directly observing the full relaxation of a single polymer.

A number of technical developments have allowed us to observe and manipulate single polymers. We used DNA as a model polymer (13, 14); because of its large contour length (10's of micrometers), detailed observation in an optical microscope is possible. Although the molecule cannot be directly manipulated with optical tweezers (15), a bead on the end of the DNA can be controlled quite easily (16). Molecular biology techniques facilitated the attachment of the DNA to a micrometer-sized bead, and highly efficient, fluorescent dyes (17) allowed us to directly visualize the molecules

in an optical microscope. In recent experiments on single DNA molecules, Smith *et al.* (18) used magnetic beads to measure the elasticity of a DNA molecule, and Matsuzaki *et al.* (19) found quantitative agreement of the rotational relaxation time with predictions of the Zimm model by observing the diffusion of single DNA molecules.

We used DNA that was 4 to 43  $\mu\text{m}$  long; molecules larger than 16  $\mu\text{m}$  were formed from several  $\lambda$ -phage DNA ( $1.9 \times 10^6 \text{ g mol}^{-1} \mu\text{m}^{-1}$ ). The variation in DNA length was probably a result of the shearing of the DNA attached to beads during pipetting. Single DNA molecules were attached to a 1.0- $\mu\text{m}$  polystyrene sphere by a streptavidin-biotin bond (20). The molecules were observed in an aqueous buffer with a viscosity of about 15 centipoise (cP) (measured by a Brookfield cone-plate viscometer) consisting of either a sucrose or a glycerol solution with 10 mM tris-HCl (pH 8), 1 mM EDTA, and 10 mM NaCl. At this ionic strength, DNA has a persistence length (a measure of polymer stiffness) of about 50 nm (13).

The optical tweezer was made by focusing a 100-mW yttrium-aluminum-garnet-Nd laser beam through a Zeiss  $\times 63$  microscope objective with a numerical aperture of 1.4. The DNA was stained with YOYO-1 (Molecular Probes, Inc.), a fluorescent dye that emits in the green por-

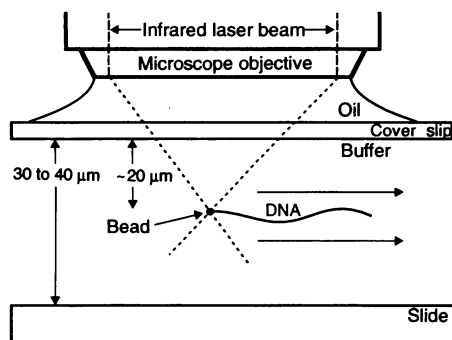


**Fig. 1.** Schematic of the apparatus. A single latex microsphere is optically trapped about halfway between the slide and cover slip in a sample with a thickness of 30 to 40  $\mu\text{m}$ . A single molecule of DNA attached to the bead is stretched to its full extension in a fluid flow and is then allowed to relax. The stained DNA was imaged with video-enhanced fluorescence microscopy.

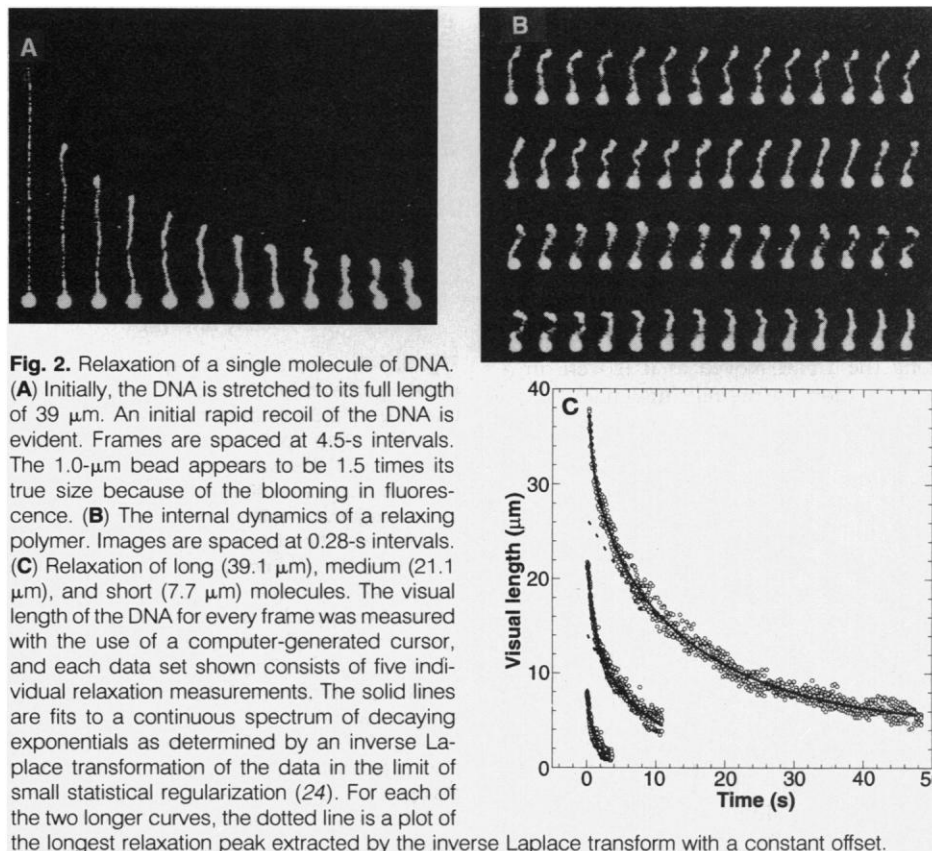


**Fig. 2.** Relaxation of a single molecule of DNA. (A) Initially, the DNA is stretched to its full length of 39  $\mu\text{m}$ . An initial rapid recoil of the DNA is evident. Frames are spaced at 4.5-s intervals. The 1.0- $\mu\text{m}$  bead appears to be 1.5 times its true size because of the blooming in fluorescence. (B) The internal dynamics of a relaxing polymer. Images are spaced at 0.28-s intervals. (C) Relaxation of long (39.1  $\mu\text{m}$ ), medium (21.1  $\mu\text{m}$ ), and short (7.7  $\mu\text{m}$ ) molecules. The visual length of the DNA for every frame was measured with the use of a computer-generated cursor, and each data set shown consists of five individual relaxation measurements. The solid lines are fits to a continuous spectrum of decaying exponentials as determined by an inverse Laplace transformation of the data in the limit of small statistical regularization (24). For each of the two longer curves, the dotted line is a plot of the longest relaxation peak extracted by the inverse Laplace transform with a constant offset.

tion of the spectrum when excited by 488-nm light from an argon-ion laser (21). To stretch the DNA, we used a feedback-stabilized motor (Oriel) to move the microscope stage at a constant velocity and generate a fluid flow around the trapped, stationary bead (Fig. 1). A flow velocity of 20  $\mu\text{m/s}$  was chosen to fully stretch the DNA. The fluorescent images were recorded by a silicon-intensified target camera (Hamamatsu C2400-08), processed by an image processor (Hamamatsu Argus 10), and digitized by a Quick Capture board (Data Translation, Marlborough, Massachusetts) at a maximum rate of 15 frames per second.

We measured the length ( $L$ ) of each stained DNA molecule by recording five video frames before the motor was turned off and measured the relaxation time of the fluid flow ( $\sim 0.1$  s) by observing the motion of a trapped bead immediately after the motor was stopped. After the flow stopped, video frames were digitized until the chain was near equilibrium. Relaxation measurements were repeated three to five times for each molecule. There was a rapid recoil of the free end to about 70% of its full length, followed by a slower relaxation (Fig. 2A). In part, such a fast initial relaxation might have been expected from static force measurements of elongated DNA, which showed a highly nonlinear dependence of the force on length at  $>75\%$  extensions (18, 22).

The relaxing end of the DNA sometimes formed a compact ball about 0.5 to 1.0  $\mu\text{m}$  in diameter (Fig. 2A). Similarly, as the chain was stretched in a flow, a coiled section usually appeared to unravel from the stretching end. This behavior may be qualitatively similar to that of the yo-yo model proposed by Ryskin (23). The video pictures also reveal fluctuations in the relaxing polymers (Fig. 2B). In addition, possible evidence for knots within a single molecule of DNA has been observed: A spot of increased fluorescence intensity along the DNA moved as if it were in a fixed location on the relaxing chain.

We used two model-independent methods to analyze the data. One method fit for a spectrum of exponential decays (Figs. 2C and 3) with an inverse Laplace transform algorithm developed by Provencher (24). The inversion of noisy data is generally not unique and using statistical regularization one finds a family of acceptable solutions as a function of the regularization parameter. For our data, discrete peaks were always present in the spectra, and in the limit of small regularization, they were very sharp, essentially corresponding to a discrete sum of exponentials. The longest relaxation times follow a scaling law with chain length  $\tau \sim L^{3\nu}$  (Fig. 3B). The scaling exponent

$3\nu$  was measured to be  $1.66 \pm 0.10$  in limit of small regularization and  $1.60 \pm 0.10$  for the broader spectra chosen by Provencher's algorithm.

The classical theories of chain dynamics such as the Rouse and Zimm models are based on the notion of normal modes of relaxation, which arise as solutions to linearized equations of motion (3, 8). Both models are statistical in nature and describe small fluctuations about equilibrium. Our experiment starts with a polymer at full extension and we expect neither model to describe the resulting relaxation. However, for lack of a theoretical framework in which to analyze the dynamics of highly extended chains, we compare our results to the Rouse and Zimm models. As pointed out by de Gennes (2), it is not clear that the concept of modes would remain valid without the simplifying assumptions in these models. The mode picture predicts sharp peaks in the decay spectrum, but the actual spectrum for dilute chains has been difficult to obtain experimentally because of the weak signals involved in standard experiments. De Gennes hypothesized that nonlinearities—from the hydrodynamic interaction, from the excluded volume interaction, and

possibly from knot formation—would tend to broaden peaks in the decay spectrum. For these reasons, he was not certain that distinct peaks would even appear in the spectrum (2).

Although our analysis does show distinct peaks in the spectrum, the structure of the spectrum was not in agreement with the mode structure of the Rouse or the Zimm model. Experimentally, the ratio of the decay times for the first to the second peak in the spectrum was  $8.3 \pm 3.2$ , and the ratio of their amplitudes was  $2.0 \pm 0.8$ . These decay times are consistent with the Rouse prediction of  $\tau_p \sim \tau_1/p^2$  and the Zimm prediction of  $\tau_p \sim \tau_1/p^{3\nu}$ , where for both predictions  $p = 1, 3, 5 \dots$  (25). However, the ratio of the amplitudes is in clear disagreement with the predicted value of 9 from the dependence of  $c_p \sim c_1/p^2$  for both the Rouse and the Zimm model. On theoretical grounds, this is not surprising because these models describe polymers fluctuating near equilibrium, and their approximations break down for large chain extensions.

Although the peaks in the relaxation spectrum do not agree with the Rouse or the Zimm theory, the last one-third of the relaxation is well fit by the longest peak in

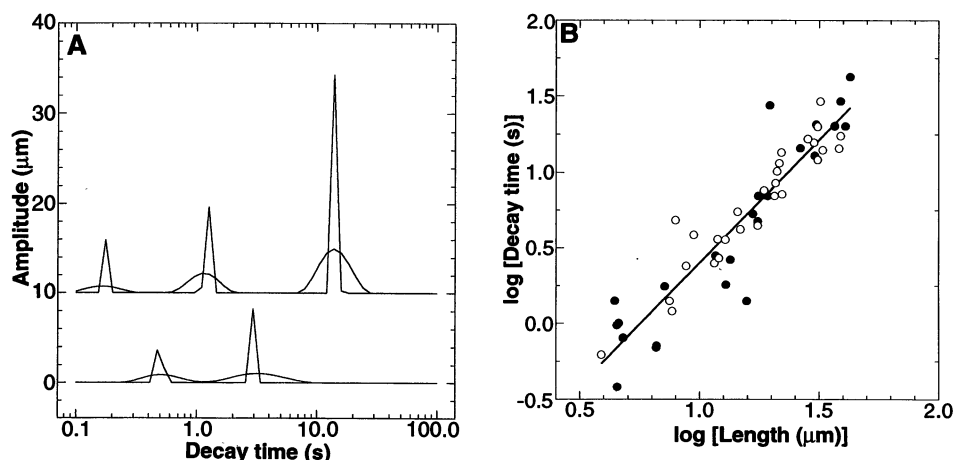


**Fig. 3:** The spectrum of decaying exponentials describing each data set was determined by an inverse Laplace transformation of the relaxation data. **(A)** Spectra for chain lengths of 38.3  $\mu\text{m}$  (top trace) and 12.8  $\mu\text{m}$  (bottom trace) in the 15-cP glycerol solution. The spectrum for the 38.3- $\mu\text{m}$  chain is shifted up by 10  $\mu\text{m}$  for clarity. The inverse Laplace transforms were computed with an algorithm (24) that determines a fit on the basis of a weighted least squares estimator with an added quadratic form as a statistical regularizer. The amplitudes of the exponentials were constrained to be nonnegative. As the regularization parameter  $\alpha$  is increased, the fit is biased toward smoother spectra, and the algorithm searches for the simplest solution consistent with the data but without overinterpretation. For much of our data, the number and position of peaks did not change as  $\alpha$  was increased; they merely broadened, indicating that these decay components were robust. In such cases, the simplest solutions would be the ones for small  $\alpha$ . However, in about a third of our data sets, some pairs of peaks merged as  $\alpha$  was increased, leaving us with a higher degree of uncertainty in the decay times. The sharp peaks are the spectra in the limit where  $\alpha$  is small ( $\alpha = 1.3 \times 10^{-8}$  for the 38.3- $\mu\text{m}$  chain and  $7.9 \times 10^{-7}$  for the 12.8- $\mu\text{m}$  chain), and the broader curves are the chosen solutions (with  $\alpha = 4.3 \times 10^{-4}$  for the 38.3- $\mu\text{m}$  chain and  $8.4 \times 10^{-4}$  for the 12.8- $\mu\text{m}$  chain). **(B)** Scaling of the longest decay times ( $\tau$ ) with length for the chosen solutions. The data were taken in (●) a sucrose solution and (○) a glycerol solution. The solid line is a linear fit to all of the data and yielded a slope of  $1.60 \pm 0.10$ . A similar analysis in limit of small  $\alpha$  gives a slope of  $1.66 \pm 0.10$ . These fits demonstrate dynamical scaling of  $\tau$  with length, and the slopes correspond to scaling exponents. The scaling exponent for the next-to-longest peak in the spectrum was  $1.4 \pm 0.2$ .

the relaxation spectrum (Fig. 2C). This may indicate the region in which agreement with the Rouse or the Zimm model would be expected because the elasticity of the chain is linear (18, 22) and well modeled as a spring that obeys Hooke's law.

Data collapse, the other method we used to measure scaling relations without reference to a specific model, is based on the similarity between the curves of the data (Fig. 4). In the data collapse method, the

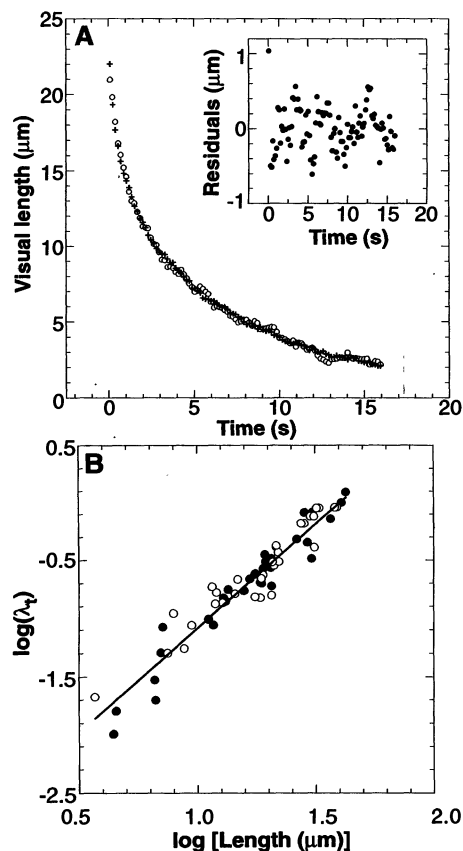


**Fig. 4.** The data collapse analysis investigated the scaling properties of the data in a model-independent manner by rescaling both the length and time axis of a chosen template data set as well as offsetting the baseline to minimize the difference between the template and each of the other data sets. The error function used to determine the fit was the sum of the mean square deviations and was implemented according to Powell's method (27). **(A)** The template data from a 42- $\mu\text{m}$  chain were rescaled to a data set for a 21- $\mu\text{m}$  chain, yielding a time rescaling parameter ( $\lambda_t$ ) of 0.31. The rescaled curves lie on top of each other quite well. **(Inset)** The difference between the two curves. **(B)** Dependence of the time rescaling parameter ( $\lambda_t$ ) on length. The data were taken in (●) the sucrose solution and (○) the glycerol solution. The solid line, a linear fit to all of the data, yielded a scaling exponent of  $1.79 \pm 0.08$ . For template sizes of 11  $\mu\text{m}$  and 23  $\mu\text{m}$ , the scaling exponents were  $1.52 \pm 0.05$  and  $1.63 \pm 0.05$ , respectively. The linear behavior of the data shows dynamical scaling in agreement with the results shown in Fig. 3B.

relaxation data are rescaled in time and length as well as a baseline offset until it lies on top of a template curve. The time rescaling parameter ( $\lambda_t$ ) then indicates how the relaxation time scales with length as the template is collapsed on to each of the other data sets.

Three templates of varying length were arbitrarily chosen and collapsed onto the rest of the data. The time rescaling parameter for the longest template ( $L = 41 \mu\text{m}$ ) (Fig. 4B) fits a scaling law  $\lambda_t \sim L^{3\nu}$  with an exponent  $3\nu = 1.79 \pm 0.08$ . The medium length template ( $L = 20 \mu\text{m}$ ) gave  $3\nu = 1.68 \pm 0.05$ , and the shortest template ( $L = 11 \mu\text{m}$ ) gave  $3\nu = 1.53 \pm 0.05$ . The longer templates may be more indicative of the true value of the scaling exponent because the data for longer pieces of DNA were better and contained more information. These scaling exponent values are consistent with the results obtained from the inverse Laplace transforms and are within the theoretical values discussed above. The systematic dependence of the exponent on template length may suggest that dynamical scaling might not be perfect but may simply be attributable to the floating baseline (especially for the shorter lengths of DNA), causing the fitting program to trade off time rescaling for baseline rescaling.

The relaxation of a tethered chain is not the same as that of a free chain. In fact, the tethered relaxation is that of a free chain of twice the length, considering symmetry about the center of mass and neglecting hydrodynamic interactions between the two halves. We have not measured the end-to-end distance of the polymer chain, rather its visual length within the depth of field of the microscope ( $\sim 1 \mu\text{m}$ ). From an experimental point of view, the difference between this relaxation and that of the end-to-end separation is probably not very significant, for the transverse excursions are almost always less than 10% of the chain length. Also, a computer simulation of the Zimm model showed that the maximum displacement (visual length) under traction was within about 2% of the end-to-end displacement for displacements above the radius of gyration.

We have measured the relaxation of a single chain from full extension. Although a highly extended chain will be in a different regime of dynamics from most theories of polymer dynamics that treat small fluctuations about equilibrium, our data agree well with dynamical scaling when both the longest relaxation ( $\tau$ ) and the rescaling parameter ( $\lambda_t$ ) are plotted on a log-log plot versus length. Our two average values of the scaling exponent agree even though the inverse Laplace transform analysis determined the scaling for the longest decay

time, which described approximately the last third of the relaxation curve, and the data collapse method, which rescaled the full relaxation curve. Our measured value of the scaling exponent of  $3\nu = 1.65 \pm 0.12$  also agrees quantitatively with the scaling exponent measured by intrinsic viscosity ( $3\nu = 1.65$ ) (11) and dynamic light scattering ( $3\nu = 1.65$ ) (6, 7) but disagrees with the birefringence measurements ( $3\nu = 1.5$ ) (5). The scaling exponent determined from an extended chain is closer to that predicted by the Zimm model, where hydrodynamic coupling within the chain is included, than that predicted by the Rouse model, where such intrachain hydrodynamic coupling is neglected. This is in disagreement with the expectation that the Rouse model is a better description than the Zimm model for extended chains (26).

## REFERENCES AND NOTES

1. P. Flory, *Statistical Mechanics of Chain Molecules* (Interscience, New York, 1969).
2. P. G. de Gennes, *Scaling Concepts in Polymer Physics* (Cornell Univ. Press, Ithaca, NY, 1979).
3. M. Doi and S. Edwards, *The Theory of Polymer Dynamics* (Clarendon, Oxford, 1986).
4. P. G. de Gennes, *Macromolecules* **9**, 587 (1976); *ibid.*, p. 594; (2).
5. A. Keller and J. Odell, *Colloid Polym. Sci.* **263**, 181 (1985); K. Narh, J. Odell, A. Keller, *J. Polym. Sci. B* **30**, 335 (1992).
6. M. Adam and M. Delsanti, *J. Phys. Paris* **37**, 1045 (1976); *Macromolecules* **10**, 1229 (1977).
7. Y. Tsunashima, N. Nemoto, M. Kurata, *Macromolecules* **16**, 584 (1983); *ibid.*, p. 1184; N. Nemoto *et al.*, *ibid.* **17**, 425 (1984).
8. P. E. Rouse, *J. Chem. Phys.* **21**, 1272 (1953); B. H. Zimm, *ibid.* **24**, 269 (1956).
9. J. Brandrup and E. Immergut, Eds., *Polymer Handbook* (Wiley, New York, 1989).
10. M. Menasveta and D. A. Hoagland, *Macromolecules* **24**, 3427 (1991).
11. D. M. Crothers and B. H. Zimm, *J. Mol. Biol.* **12**, 525 (1965).
12. J. des Cloizeaux, *J. Phys. Lett. Paris* **39**, 99 (1978).
13. P. J. Hagerman, *Annu. Rev. Biophys. Biophys. Chem.* **17**, 265 (1988).
14. R. Pecora, *Science* **251**, 893 (1991).
15. A. Ashkin, J. Dziedzic, J. Bjorkholm, S. Chu, *Opt. Lett.* **11**, 288 (1986).
16. Earlier work was reported by S. Chu [*Science* **253**, 861 (1991)] and S. Chu and S. Kron [*International Conference on Quantum Electronics Technical Digest* (Optical Society of America, Washington, DC, 1990), vol. 8, p. 202. See also the accompanying paper by T. T. Perkins, D. E. Smith, and S. Chu [*Science* **264**, 819 (1994)].
17. H. S. Rye *et al.*, *Anal. Biochem.* **208**, 144 (1993).
18. S. B. Smith, L. Finzi, C. Bustamante, *Science* **258**, 1122 (1992).
19. M. Matsumoto *et al.*, *J. Polym. Sci. Polym. Phys. Ed.* **30**, 779 (1992).
20. A 28-base pair (bp) oligonucleotide (Stanford University Protein and Nucleic Acid Facility, Stanford, CA) was ligated on to the  $\lambda$ -phage DNA (Gibco BRL), leaving a specific 16-bp overhang on one end. A biotinylated oligonucleotide complementary to this 16-bp overhang was attached to the streptavidin-coated bead. The modified DNA was then attached to these beads by hybridization.
21. To reduce photobleaching of the dye, we enzymatically scavenged oxygen with glucose oxidase (50  $\mu\text{g}/\text{ml}$ ), 0.1% glucose, and catalase (10  $\mu\text{g}/\text{ml}$ ) (Sigma), as in A. Kishino and T. Yanagida, *Nature* **334**, 74 (1988).

22. T. T. Perkins, S. R. Quake, D. E. Smith, S. Chu, unpublished results.
23. G. Ryskin, *J. Fluid Mech.* **178**, 423 (1987).
24. S. W. Provencher, *Comput. Phys. Commun.* **27**, 213 (1982).
25. The symmetry of the tethered chain yields only the odd modes within these models. The amplitudes for the Zimm model are approximate and are given in B. H. Zimm, G. M. Roe, L. F. Epstein, *J. Chem. Phys.* **24**, 279 (1956). The values reported are the average of the two solutions from the inverse Laplace transform. The ratios for the solution chosen by Provencher's algorithm were  $10.1 \pm 4.0$  for the times and  $2.3 \pm 0.9$  for the amplitudes. The corresponding values in the limit of small regularization are  $6.4 \pm 2.0$  and  $1.7 \pm 0.7$ .
26. P. G. de Gennes, *J. Chem. Phys.* **60**, 5030 (1974).
27. W. H. Press *et al.*, *Numerical Recipes* (Cambridge Univ. Press, Cambridge, 1989), pp. 309–317.
28. We acknowledge the generous assistance of J. Spudich and his colleagues, J. Finer, H. Goodson, and G. Nuckolls, including support through National Institutes of Health grant 33289 to J. Spudich. We also acknowledge the introduction to biochemistry given to S.C. by S. Kron, discussions with G. Fuller, R. Larson, R. Pecora, Y. Rabin, R. Stinchcombe, and B. Zimm, and the computer code and advice of S. Provencher. This work was supported in part by grants from the U.S. Air Force Office of Scientific Research and the National Science Foundation and by an endowment established by Theodore and Frances Geballe.

29 December 1993; accepted 1 April 1994

## Surface Vibrational Spectroscopic Studies of Hydrogen Bonding and Hydrophobicity

Quan Du, Eric Freysz,\* Y. Ron Shen†

Surface vibrational spectroscopy by sum-frequency generation was used to study hydrophobicity at the molecular level at various interfaces: water–surfactant-coated quartz, water–hexane, and water–air. In all cases, hydrophobicity was characterized by the appearance of dangling hydroxyl bonds on 25 percent of the surface water molecules. At the water–quartz interface, packing restrictions force the water surface layer to have a more ordered, ice-like structure. A partly wettable water–quartz interface was also studied.

Knowledge about interfacial water structure near hydrophobic surfaces is crucial for the understanding of many important surface problems involving water. For instance, wetting or nonwetting is a familiar phenomenon, but there is not yet a clear physical picture of the phenomenon at the molecular level (1). Hydrophobic interactions are responsible for the formation of micelles (2) and play an important role in organizing constituent molecules of living matter into complex structures such as membranes (2, 3). The understanding of hydrophobic interfaces can also provide a better picture of how hydrophobic solute particles are surrounded by water molecules when immersed in water (4). In the past, the importance of such interfaces has stimulated a number of theoretical studies done with numerical calculations (5–7). Experimental research on the topic, however, has been rare or nonexistent because of a lack of suitable techniques. Recently, infrared-visible sum-frequency generation (SFG) has been developed into a versatile surface spectroscopic tool that can be used to probe all types of interfaces, including liquid-liquid and solid-liquid interfaces (8–10).

Department of Physics, University of California, and Materials Sciences Division, Lawrence Berkeley Laboratory, Berkeley, CA 94720, USA.

\*Present address: Centre de Physique Moléculaire, Université de Bordeaux 1, 351 Avenue de la Libération, 33405 Talence CEDEX, France.

†To whom correspondence should be addressed.

We report vibrational spectroscopic measurements made on two hydrophobic interfaces. One was a water–solid interface, where the solid surface was rendered hydrophobic by a monolayer coating of surfactant OTS [octadecyltrichlorosilane,  $\text{CH}_3(\text{CH}_2)_{17}\text{SiCl}_3$ ], and the other was a water–hexane interface. The spectra were compared with that of the water–air interface, which can also be regarded as hydrophobic. In all cases, the hydrophobic interaction was characterized by the appearance of a free hydroxyl (OH) stretch peak of

water in the spectra. The bonded OH spectra of water at the different interfaces showed some clear differences, which suggested a difference in the water's interfacial structure. The water molecules against the solid wall appeared to be more bond-ordered. We also probed a partly wettable surface prepared by a monolayer coating of surfactants that had loosely packed hydrocarbon chains. No free OH peak was observed in that case.

The SFG technique has been described previously (8). Within the electric dipole approximation, the process is forbidden in a centrosymmetric bulk medium such as water but allowed at the surface, where the inversion symmetry is broken. For water interfaces, it has been shown (9) that the quadrupolar contribution from the bulk water is not appreciable and that the SFG in reflection comes mainly from the dipolar contribution of interfacial water molecules with preferred polar orientations.

The experimental setup for our SFG measurement has also been described elsewhere (8, 11). The hydrophobic solid surface was prepared by depositing a monolayer of OTS on the surface of a fused quartz window by means of a standard self-assembly technique (12). The hydrophobicity of the surface came from the layer of closely packed hydrocarbon chains. The SFG spectrum in the OH stretch region that was obtained from this quartz–OTS–water interface is shown in Fig. 1A. The sum-frequency (SF) output, visible input, and infrared (IR) input were s-, s-, and p-polarized, respectively (denoted by ssp). The results were similar to those obtained from an air–water interface (9), the ssp spectrum of which is shown in Fig. 1B for comparison. In both cases, the spectrum exhibited a sharp peak at  $3680 \text{ cm}^{-1}$  that can be assigned to the non-hydrogen-bonded OH

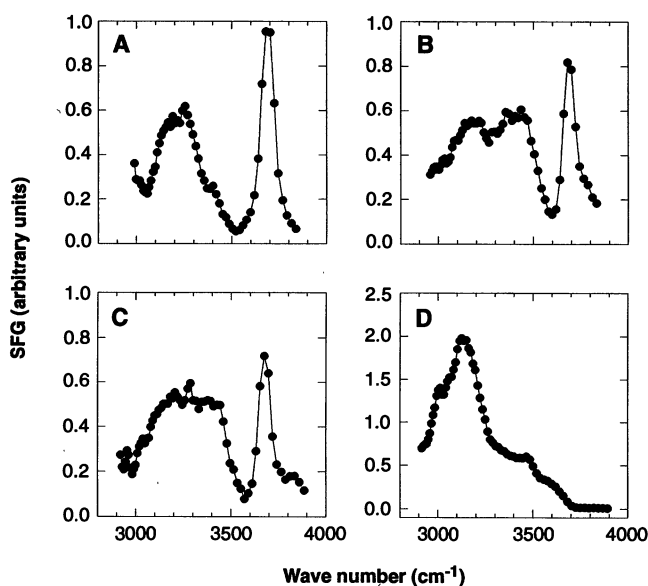


**Fig. 1.** SFG spectra from (A) the quartz–OTS–water interface, (B) the air–water interface, (C) the hexane–water interface, and (D) the quartz–ice interface. The SF output, visible input, and IR input were s-, s-, and p-polarized, respectively.